

4th International Conference on Silicon Photovoltaics, SiliconPV 2014

Micro characterization and imaging of spikes in nickel plated solar cells

Andreas Büchler*, Sven Kluska, Andreas Brand, Christian Geisler, Sybille Hopman, Markus Glatthaar

Fraunhofer Institute for Solar Energy Systems (ISE), Heidenhofstr. 2, 79110 Freiburg, Germany

Abstract

Annealing induced silicidation of plated nickel contacts can severely lower the solar cell performance due to deep nickel silicide spikes penetrating the space charge region. This work summarizes several attempts to characterize performance limiting deep silicide structures and determines the influence of different passivation layer structuring technologies on the silicide growth. Reverse biased electroluminescence measurements revealed that the deep nickel silicides occur after an anneal and are relocated along the structured and plated passivation layer openings. Cross-section studies of the plated contacts demonstrated that deep silicide growth is present independently of the applied passivation layer structuring technology. While for laser-ablation the critical silicide structures could be mostly attributed to accelerated silicide growth at laser induced defects, there are also deep silicide structures that appear without any obvious correlation even in the case of defect free wet chemical passivation structuring of the contact openings. By varying the emitter doping profile and the annealing temperature after plating the distance of the space charge region and the surface was found to influence the annealing-induced solar cell performance decrease. Considering the presented results there are three ways to overcome annealing induced degradation of Ni plated solar cells. Either optimized process designs with sufficient contact adhesion and contact resistivity without the need of thermal silicide formation, improved silicide depth control (e.g. Ni source limited growth) or the implementation of a selective emitter design with pn-junction depths well above 1 μm within the contacted area .

© 2014 Published by Elsevier Ltd. This is an open access article under the CC BY-NC-ND license (<http://creativecommons.org/licenses/by-nc-nd/3.0/>).

Peer-review under responsibility of the scientific committee of the SiliconPV 2014 conference

Keywords: nickel silicide, selective emitter, laser ablation, nickel plating, ReBEL

* Corresponding author. Tel.: +49 761 4588 5598
E-mail address: andreas.buechler@ise.fraunhofer.de

1. Introduction

Plated nickel-copper contacts may be a valuable alternative to screen printed silver in industrial manufacturing of high efficiency solar cells [1]. The formation of a Ni-silicide layer at the contact interface can significantly increase the contact adhesion [2] and contact resistivity [3]. Usually, the formation is induced in a thermal annealing process featuring temperatures of 250-450°C. This temperature range is connected to the formation of Ni₂Si and NiSi silicide phases [4]. The growth of local nickel-silicide structures with a depth comparable to the distance between surface and space charge region induce recombination active breakdown sites that lower the global electrical performance in the solar cell [5, 6]. This degradation is most prominent in the decrease of the pseudo fill factor. Due to their twofold impact in forward and reverse bias, the structures that lower the solar cell performance can be visualized via reverse-biased electroluminescence. This insight allowed the localization of the Ni spikes and the analysis of different process variables regarding their impact on the formation of critical nickel spikes. The presented study is based on reverse-biased-electroluminescence imaging, pseudo fill factor measurements by SunsV_{oc} [7] and electro-microscopic cross section analysis. Whereas Tous *et al.* [8] described nickel silicide may also be formed by excimer laser annealing, this work focuses on silicidation via thermal annealing. The evaluation of relevant processing variables included three different emitter doping profiles, four annealing temperatures for the silicide formation and four structuring techniques for contact opening formation of the passivation layer.

2. Solar cell fabrication

In the presented work the influence of several process variables on the formation of the critical nickel silicide structures will be evaluated. 45 x 45 mm² Al-BSF solar cells with Ni-Ag plated contacts on the front side were fabricated using 125x125 mm² p-type mono crystalline Cz-silicon material with random pyramid texture. Each wafer featured four isolated emitter window regions with a thermally diffused emitter. The doping profile was varied to achieve pn-junction depths between 0.3 to 1 μm and therefore, a variable critical silicide depth (distance (x_{SCR}) between surface and space charge region (SCR)). The rear side features an aluminum back surface field and the front side a PECVD silicon nitride passivation layer. The passivation layer was locally removed before galvanic metallization. Light induced plating [9] was used for the local deposition of a nickel layer with a thickness of about 0.5 μm on the openings. In order to estimate the influence of the applied passivation structuring method, four different technologies were evaluated. Solar cells with a selective emitter design were realized using laser structuring methods with simultaneously doping of the structured region via laser chemical processing (LCP) [10] and wet-film-laser-doping (WFLD) [11]. Thereby, the SCR is lowered underneath the contact opening and the contact properties are enhanced due to the high doping concentration. While for LCP a green nanosecond laser (532 nm, 40 ns) was used, WFLD was performed using a continuous wave laser of the same wavelength. The alternative structuring processes without additional doping were pico second UV-laser (PS) (355 nm, 15 ps) ablation and an inkjet mask-and-etch (M&E) process. The latter one allows a local masked wet chemical removal of the the passivation layer, without the risk of laser induced crystal defects along the contact opening. The solar cells were divided in four groups that are mixed in respect to the opening method. Each group was annealed separately for 10 minutes in a forming gas atmosphere. The annealing temperature varied with the four groups from 300°C, 350°C, 400°C to 450°C. In contrast to solar cell manufacturing for the previous publications [5, 6] the annealing was performed immediately after nickel deposition.

The contact-grid design featured 45 contact fingers (1 mm pitch) and a centric busbar with a width of 1 mm. The opening width of the structured passivation layer contact openings under the contact fingers varies with the structuring techniques.

Fig.1. summarizes the basic characteristics of the four structuring technologies. The mean effective width of the passivation layer opening below the contact fingers was analysed by microscopic images of the contact. This area is crucial since it increases the area of the nickel silicide interface. Thus the propability of deep silicidation is enhanced. Fig. 1. exemplarily shows the achieved opening structures. While the opening structures of LCP and PS had a width of approx. 20 μm, M&E opening structures are clearly wider (approx. 75 μm). The WFLD-structured passivation layer opening is just 10 μm wide and not continuously realized.

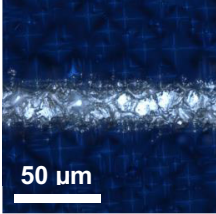
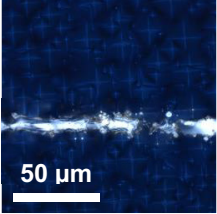
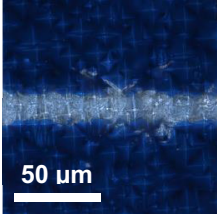
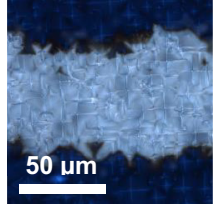
Abbreviation, technological name, structuring method			
LCP <i>Laser chemical processing</i>	WFLD <i>Wet film laser doping</i>	PS <i>Pico second pulse UV laser</i>	M&E <i>Mask & Etch</i>
laser ablation + simultaneous doping	laser ablation + simultaneous doping	Laser ablation without doping	Chemical ablation without doping
Microscope pictures of the contact openings			
			
50 μm	50 μm	50 μm	50 μm
Mean effective structuring width and mean area of silicon nickel interface			
$(23 \pm 1) \mu\text{m}$	$(10 \pm 3) \mu\text{m}$	$(18 \pm 1) \mu\text{m}$	$(76 \pm 15) \mu\text{m}$
90,54 mm ²	64,8 mm ²	80,64 mm ²	195,48 mm ²

Fig. 1. Summary of the used passivation structuring technologies.

3. Characterization of critical nickel silicide structures via imaging

As presented in previous publications the degradation of the cell performance is reflected in the pFF [5]. Throughout this work the pFF of the analyzed solar cells is measured via a Sinton SunsV_{OC} tester [7]. Furthermore, reverse biased electroluminescence (ReBEL) were applied for precise localization of the silicidation induced recombination active breakdown sites. In a microscopic ReBEL set-up a radiative breakdown site was localized up to 1 μm . Subsequent electro microscopic cross-section studies revealed deep nickel silicide structures on the very same position [6].

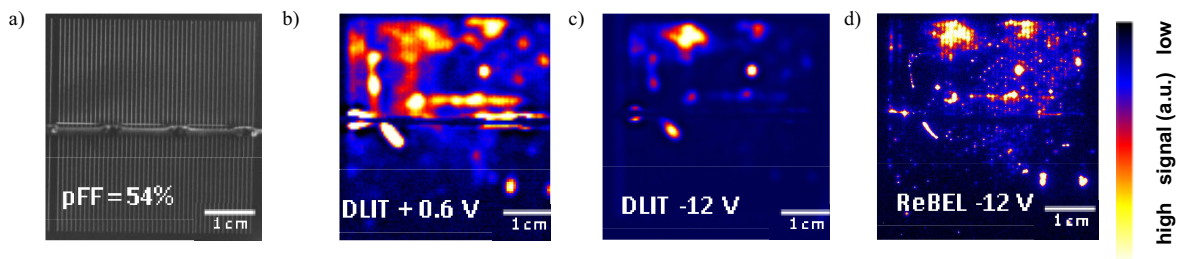


Fig. 2. (a) Monochrome image of a M&E-structured solar cell with the measured pFF after Ni silicidation at 350°C (b) 90°-DLIT-image under +0.6 V (c) 90°-DLIT-image under -12 V (d) ReBEL-image under -12 V.

Fig. 2. shows dark lock-in thermography (DLIT) and ReBEL measurements that visualize the twofold impact of nickel silicide formation in forward and reverse bias of a solar cell that was produced and evaluated within this work. The presented solar cell was structured via mask & etch. The plated nickel layer was annealed at 400°C peak temperature. Before nickel plating the pFF reached 83%, after the annealing it dropped to 54%. As shown by Kluska

et al. [5] the annealing induced pFF drop is caused by local power losses that are visible in DLIT under + 0.6 V. The DLIT and the ReBEL image at -12 V shows local breakdown sites by detecting the emitted heat and light radiation, respectively. The very same structures show no measureable emission under - 0.6 V in DLIT and ReBEL (not shown here). These reproduces the observations that were published for LCP-structured solar cells [6]. Due to the thermal diffusion the spatial resolution of DLIT measurements is limited. For the characterization of nickel silicide spikes, ReBEL measurements are more suitable to evaluate the amount and distribution of the performance limiting structures.

4. Passivation structuring induced silicidation characteristics

4.1. Annealing induced pFF decrease

Fig. 3. shows the results of pFF measurements before and after annealing. The diagram is separated in several sections by dashed lines. The first section shows the pFF -values before annealing. Each further section exhibits the results of the several annealing groups. The sections are labeled with the respective process temperature. Within each section the pFF -values are clustered according to the associated passivation structuring technology. The different structuring methods are color coded. Box-plots facilitate the comparison of the pFF -distributions.

With increasing process temperature the distributions of measured pFF -values shifts to lower values. The comparison of the different structuring techniques reveals that the structuring technology systematically influences the temperature dependence of the pFF -decrease.

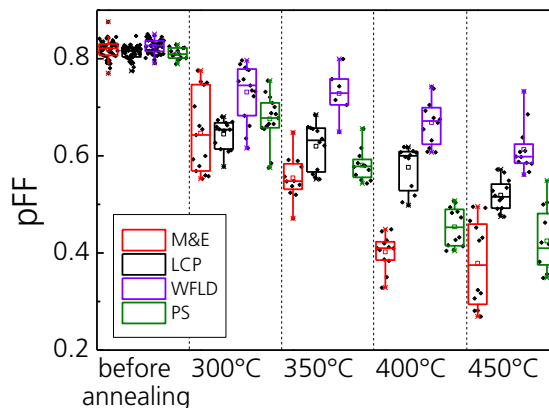


Fig. 3. Results of pFF -measurements of all solar cells including the three different emitter doping profiles. The section on the very left side shows the pFF -level before annealing for solar cells structured by different techniques. The other sections refer to the four process temperatures. For each temperature the results are grouped according to the associated structuring method

As Fig. 3 indicates, the mean pFF of the solar cells structured by the same particular technology was 82 % before annealing. Due to annealing the pFF severely decreases for all solar cells at all studied temperatures. Further, for all four structuring methods higher annealing temperatures led to lower pFF . For any temperature the results after anneal shows a clear dependence on the structuring method.

The decrease is less severe on solar cells featuring selective emitter (LCP, WFLD). WFLD structured solar cell exhibited the highest pFF values within all temperature groups. This may be attributed to the deep doping ($x_{SCR} = 3.5\text{-}5\ \mu\text{m}$) below the opening. The undoped PS-structures reveal higher pFF values as LCP-structured solar cells for an annealing temperature of 300°C. It is reasonable that laser defects promote deep silicidation on LCP cells. Within the three groups that had been annealed in temperatures higher than 300°C LCP-structured solar cells generated higher pFF -values compared to undoped openings. This indicates that additional doping ($x_{SCR} = \text{approx.}1.5\ \mu\text{m}$) may partially compensate laser induced defects. Comparing the structuring method without additional doping PS structured solar cells show higher pFF -values than M&E-structured solar cells throughout the

whole temperature range. A reason may be the different opening widths. M&E structures are wider than PS structures. Therefore, the area that is beset with nickel is larger on M&E structures. If deep silicidation is caused by defects on the wafer, the probability that these defects lie within the nickel-silicon interface is higher on M&E-structured cells.

4.2. Reverse biased electroluminescence imaging of silicide spikes

Fig. 4. shows superpositions of ReBEL-images and monochromatic pictures of four solar cells. The solar cells were annealed at 400°C and featured different passivation structuring methods. All measurements were performed under an applied voltage of -15 V.

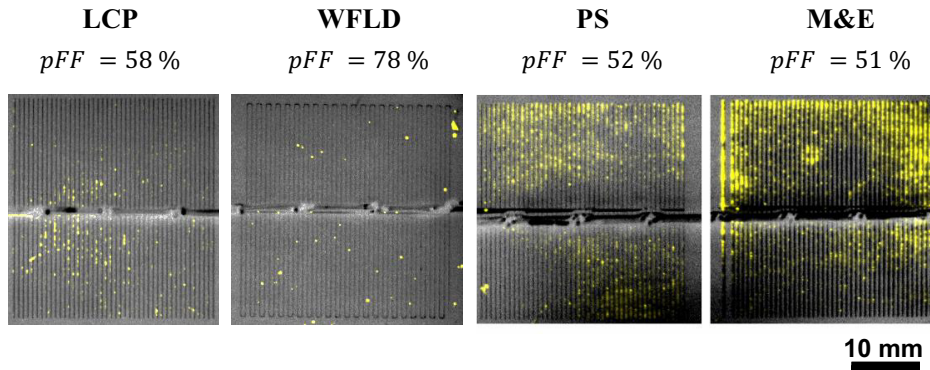


Fig. 4. Superpositions of monochromatic images of different solar cells with different passivation structuring techniques and the according ReBEL-image (yellow) that shows radiative breakdown sites. The busbar is in the shown measurements shadowed by the contact rail of the voltage source. The 45 x 45 mm² solar cells were manufactured on the same wafer, that was tempered at 400°C after nickel plating.

The ReBEL images show less amounts of radiative breakdown sites for solar cells with selective emitter design (LCP, WFLD). The comparison of *pFF*-results and ReBEL images reveal the expected correlation. The more breakdown sites occur, the more intensive is the *pFF*-decrease due to silicide formation. There is no characteristic difference between the UV-laser structured solar cell and the mask-and-etch structured solar cells. The ReBEL measurements underline that deep nickel silicide growth is highly localized to some 10 to 1000 structures on the wafer area.

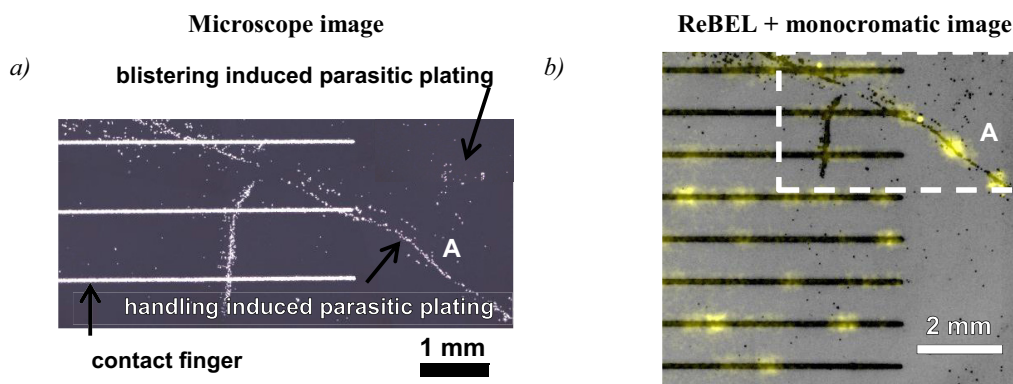


Fig. 5. (a) Microscope image of a solar cell surface with increased parasitic-plating (b) superposition of monochromatic image (grey) and ReBEL image (yellow). The dashed lines mark the region of the image in a).

Microscopic pictures reveal parasitic plated areas on the solar cell surface (Fig. 5. (a)). Due to handling induced scratches and blistering of the passivation layer Nickel was deposited outside the structured areas. In order to evaluate if the spots of parasitic deposited nickel may form critical silicide an area of increased ghost-plating was measured with ReBEL. Fig. 5. (b) shows an ReBEL-image with enhanced resolution. It is overlaid with an monochromatic image (grayscale). The black lines represent the contact fingers. The black dots are ghost-plating spots. The ReBEL signal (yellow) was measured at -10 V. Light emitting breakdown sites are located along the opening structures, while most ghost-plating spots do not cause early breakdown. Nevertheless, there are spots with ghost-plating that influence the electrical characteristics (region A). On these spots parasitic-plating is combined with a scratch in the passivation layer. Therefore, ReBEL showed parasitic-plating may influence the electrical properties when it is located at a defect structure. But the dominant structure that is harmed by silicidation are the contact openings. To investigate the silicidation along the opening structures SEM studies were conducted along cross-sections.

4.3. SEM cross-section analysis of critical silicide structures

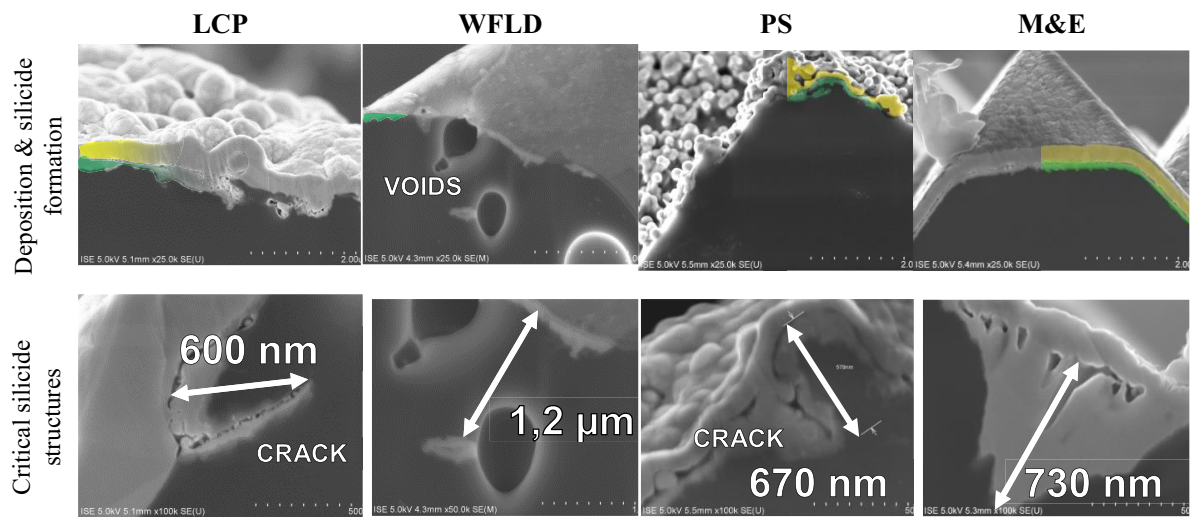


Fig.6. SEM images of cross sections along the opening region after plating and a subsequent annealing step of 400°C . Each column represents a different structuring method. The first row shows the typical shape of the deposited nickel layer (partly colorized in yellow) and the formed silicide layer (partly colorized in green). The second row highlights critical nickel silicide structures for the particular structuring technology.

After the electrical characterization cross sections were prepared by ion polishing for SEM studies. All shown samples were cut out of the same wafer, which was annealed at 400°C after plating. For each structuring method Fig. 6. shows two images. The first picture represents the typical shape of the deposited nickel layer (partly colorized in yellow) and the silicide formation along the surface (partly colorized in green). The shape of the nickel silicide layer is different for each passivation structuring method. But within each cross section sample the particular depth is quite homogeneous. In several similar cross section studies typical deep silicide structures were found for all structuring methods. For each structuring technology one representative critical silicide structure is shown in the second row of Fig. 5. For LCP and PS structured contact opening regions, silicon micro cracks were found, which are typical structures of accelerated silicide growth [12, 13]. Voids occur along the WFLD-opening structure. The bubble-shaped cavities are observed in various depths and with various diameters. The arrangement of the voids that are visible on any cross-section sample, follows patterns that can be attributed to the convection motions of molten silicon (A detailed discussion will be published elsewhere). Nickel silicides are frequently detected in their surroundings. The correlation between local defect structures and enhanced Ni silicide growth is known from the literature as Ni encroachment [12-14]. Thus, laser induced defects of the different passivation structuring

techniques propagate deep local silicide growth. Accelerated silicide growth at defect structures can also be an explanation why local breakdown sites at parasitic plated regions occur mostly in regions of handling induced scratches and only in minor amounts in blistering induced regions. Nevertheless, mask and etch structured openings that are supposed to feature an almost defect free contact opening show deep silicide structures, too. These pyramidal shaped deep spikes that locally grow five times deeper than the homogeneous silicide layer in their immediate vicinity, harm the local electrical properties of the solar cell.

5. Emitter depth dependence of silicidation induced pFF degradation

The comparison of different structuring methods with regard to the pFF -results after annealing at temperatures higher than 300°C revealed that solar cells with selective emitter design showed higher values than cells without additional doping. It was assumed that the local lowering of the SCR beneath the contacts may minimize the influence of nickel silicide spikes. Since the effect of deep nickel silicides on the cell performance is more severe if the defects reach the space charge region.

In order to evaluate the influence of x_{SCR} , three different doping profiles were used in the presented experiment for the formation of the homogeneous emitter. Varying the homogeneous emitter allowed for more precise knowledge of x_{SCR} and ensured that the SCR is lower particularly beneath the opening. Electrochemical capacitance voltage (ECV) measurements revealed the three doping profiles that are plotted in Fig. 7. (a). The simulated x_{SCR} , the calculated sheet resistance (R_{sh}) and the measured pn-junction depth (x_{pn}) is stated in the same figure.

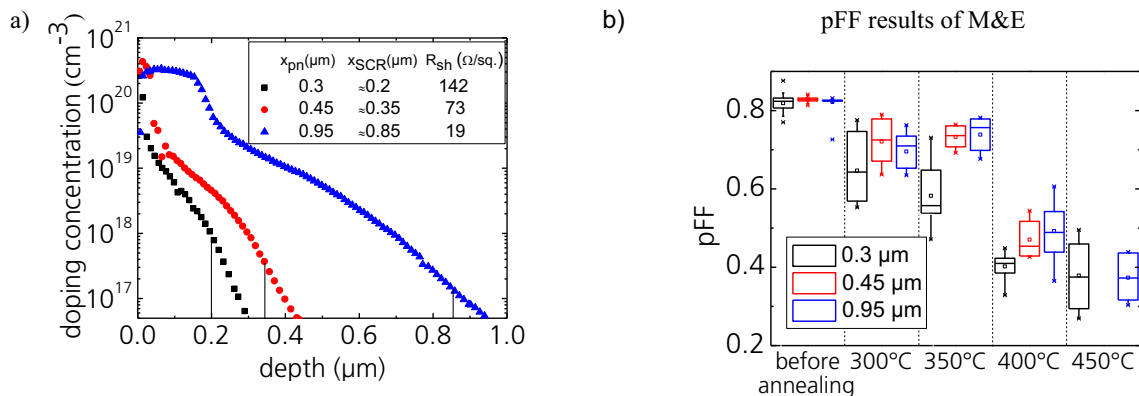


Fig. 7. (a) ECV [15] profiles of the three different thermally diffused emitters and (b) results of pFF -measurements of M&E-structured solar cells with varying doping profiles. The section on the very left side shows the pFF -level before annealing. The other sections refer to the four process temperatures. For each temperature the results are grouped according to the associated emitter profile.

Fig. 7. (b) exhibits the pFF measurements before and after annealing of solar cells that are structured by mask-and-etch. Each section represents the results of different annealing groups. The different doping profiles determine the color coding of the box-blots.

The results proves following assumption: The solar cells featuring a shallow emitter doping profile depth are the ones with the lowest pFF values in all process groups. In particular after annealing at temperatures of 350°C and 400°C the distributions of the pFF results correlates with the depth of the SCR. At 450°C all solar cells are equally damaged.

6. Conclusion

Thermal silicidation of a plated nickel layer may enhance electrical properties of plated contacts. At the same time the formation of deep local silicide structures jeopardize the solar cell performance. This work discussed

critical aspects of the silicide formation in order to identify possible failure mechanisms of Ni-Cu or Ni-Ag plated solar cell sources.

Pseudo-fill factor measurements of Ni plated solar cells demonstrated that the cell performance is severely harmed by annealing induced silicidation of the Ni-Si contact interface. Even 300°C process temperature lowers significantly the cell performance. ReBEL was used to visualize the spatial distribution of critical silicide structures. The analysis in an area with high density of parasitic-plating showed that critical silicide structures are mainly found along the contact lines. However, also handling induced damage structures of the passivation lead partly to recombination active breakdown spots. Further SEM cross-section studies of contact areas that were structured by different passivation structuring technologies were conducted. For all structuring methods a mostly homogeneous nickel silicide layer was formed along the opening. On few spots deep nickel silicide structures were found that grow up to 10 times deeper than the homogeneous layer. On laser-structured openings deep silicidation was prominently found along laser induced defects. On defect free mask-and-etch structured passivation layer openings deep single silicide structures were found, without any visible correlation to local defect structures.

In order to estimate the influence of the distance between the space charge region and the surface in comparison to the silicid depth distribution, solar cells with various emitter doping profile were compared. The results showed the decrease of the cell performance due to annealing induced silicidation depends on the emitter profile. If the distance between space charge region and surface is shallow, the impact of silicidation induced performance degradations is increased. Furthermore, this work could show that even a thermally diffused emitter profile with a pn-junction depth of 0.95 μm is not necessarily sufficient to prevent power losses due to local deep silicide structures.

In order to avoid the degradation due to silicidation we suggest the following three options. 1. Reconsider if the annealing is necessary. Appropriate opening structuring methods and plating conditions may provide the required mechanical and contact resistivity properties without annealing. Regarding the production of plated contacts for high-efficiency silicon solar cells with very lightly doped surface doping concentrations silicidation might be indispensable for the contacting. 2. The amount of deposited nickel could be reduced. The growth of deep structures could then be limited by the nickel source. 3. A selective emitter design lowers the space charge region locally and avoids the impact of deep structures on the electrical performance.

Acknowledgements

The authors would like to thank Fabian Meyer, Wilhelm Hoerdts and David Stüwe for realizing the different passivation layer openings. Further we would thank Gisela Cimiotti for plating, Matthias Weng for annealing and the ISE PV-Tec and ISE clean room team for cell manufacturing.

References

- [1] Metz, A., et al., "Industrial High Performance Crystalline Silicon Solar Cells and Modules Based on Rear Surface Passivation Technology". *Solar Energy Materials and Solar Cells*, 2014. **120**: p. 417–425.
- [2] Mondon, A., et al., "Microstructure analysis of the interface situation and adhesion of thermally formed nickel silicide for plated nickel–copper contacts on silicon solar cells". *Solar Energy Materials and Solar Cells*, 2013. **117**(0): p. 209–213.
- [3] Stavitski, N., et al., "Systematic TLM measurements of NiSi and PtSi specific contact resistance to n- and p-type Si in a broad doping range". *Electron Device Letters, IEEE*, 2008. **29**(4): p. 378–381.
- [4] Coe, D.J. und E.H. Rhoderick, "Silicide formation in Ni-Si Schottky barrier diodes". *Journal of Physics D: Applied Physics*, 1976. **9**(6): p. 965.
- [5] Kluska, S., et al., "Micro characterization of laser structured solar cells with plated Ni–Ag contacts". *Solar Energy Materials and Solar Cells*, 2014. **120**: p. 323–331.
- [6] Büchler, A., et al., "Localization and characterization of annealing-induced shunts in Ni-plated monocrystalline silicon solar cells". *Phys. Status Solidi RRL*, 2014.
- [7] Sinton, R.A., et al. "Quasi-steady-state photoconductance, a new method for solar cell material and device characterization". in *Proceedings of the 25th IEEE Photovoltaic Specialists Conference*. 1996. Washington DC, USA: IEEE; New York, NY, USA.

- [8] Tous, L., *et al.*, "Nickel silicide contacts formed by excimer laser annealing for high efficiency solar cells". *Progress in Photovoltaics: Research and Applications*, 2013. **21**(3): p. 267-275.
- [9] Bartsch, J., *et al.* "Progress in understanding the current paths and deposition mechanisms of light-induced plating and implications for the process". in *Proceedings of the 24th European Photovoltaic Solar Energy Conference*. 2009. Hamburg, Germany.
- [10] Kray, D., *et al.*, "Laser Chemical Processing (LCP)—A versatile tool for microstructuring applications". *Applied Physics A: Materials Science & Processing*, 2008. **93**(1): p. 99-103-103.
- [11] Hallam, B., *et al.*, "Record large-area p-type CZ production cell efficiency of 19.3% based on LDSE technology". *Photovoltaics, IEEE Journal of*, 2011. **1**(1): p. 43-48.
- [12] Hoummada, K., *et al.*, "Nickel segregation on dislocation loops in implanted silicon". *Scripta Materialia*, 2011. **64**(5): p. 378-381.
- [13] Hoummada, K., *et al.*, "Redistribution of arsenic during the reaction of nickel thin films with silicon at relatively high temperature: Role of agglomeration". *Microelectronic Engineering*, 2006. **83**(11-12): p. 2264-2267.
- [14] Imbert, B., *et al.*, "Nickel silicide encroachment formation and characterization". *Microelectronic Engineering*, 2010. **87**(3): p. 245-248.
- [15] Blood, P., "Capacitance-voltage profiling and the characterisation of III-V semiconductors using electrolyte barriers". *Semiconductor Science and Technology*, 1986. **1**(1): p. 7.